molecular pharmaceutics

Article

pubs.acs.org/molecularpharmaceutics

Combination Therapy of NSCLC Using Hsp90 Inhibitor and Doxorubicin Carrying Functional Nanoceria

Shoukath Sulthana, Tuhina Banerjee, Jyothi Kallu, Sudershini Reddy Vuppala, Blaze Heckert, Shuguftha Naz, Tyler Shelby, Olivia Yambem,[§] and Santimukul Santra*[,†]

[†]Department of Chemistry, Kansas Polymer Research Center, Pittsburg State University, 1701 S. Broadway Street, Pittsburg, Kansas 66762, United States

[§]Department of Neurology, College of Medicine, University of Tennessee Health Science Center, 855 Monroe Avenue, Memphis, Tennessee 38163, United States

Supporting Information

ABSTRACT: K-RAS driven non-small-cell lung cancer (NSCLC) represents a major cause of death among smokers. Recently, nanotechnology has introduced novel avenues for the diagnosis and personalized treatment options for cancer. Herein, we report a novel, multifunctional nanoceria platform loaded with a unique combination of two therapeutic drugs, doxorubicin (Doxo) and Hsp90 inhibitor ganetespib (GT), for the diagnosis and effective treatment of NSCLC. We hypothesize that the use of ganetespib synergizes and accelerates the therapeutic efficacy of Doxo via ROS production, while minimizing the potential cardiotoxicity of doxorubicin drug. Polyacrylic acid (PAA)-coated cerium oxide nanoparticles (PNC) were fabricated for the targeted combination therapy of lung cancers. Using "click" chemistry, the surface carboxylic acid groups of nanoceria were decorated with folic acid to target folate-receptor-overexpressing NSCLC. As a result of combination therapy, results showed more than 80% of NSCLC death within 48 h of incubation. These synergistic therapeutic effects were assessed via enhanced ROS, cytotoxicity, apoptosis, and migration assays. Overall, these results indicated that the targeted codelivery of Doxo and GT using nanoceria may offer an alternative combination therapy option for the treatment of undruggable NSCLC.

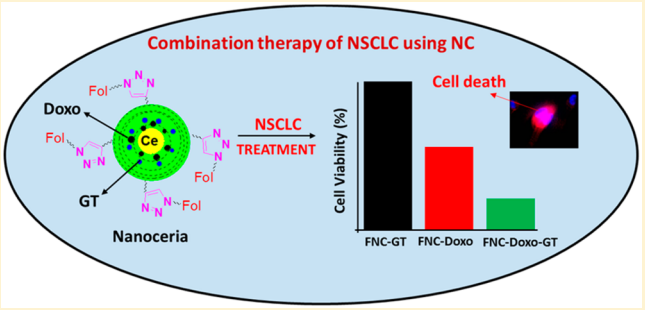

KEYWORDS: *combination therapy, NSCLC treatment, Hsp90 inhibitor, drug delivery, nanoceria, doxorubicin*

INTRODUCTION

Lung cancer is by far one of the leading cause of the mortality worldwide.[1,2] According to the American Cancer Society statistics, collectively 221 200 new cases of lung cancer and 158 040 deaths were estimated in the year 2015. Histologically, lung cancer is being classified into two major subtypes: small-cell lung cancer (SCLC) and non-small-cell lung cancer (NSCLC). Among both the subtypes, NSCLC by itself accounts for 85% of all the cases.[3] Oncogenic K-RAS, one of the major histologic subtype of NSCLC, accounts for more than 25% of the lung-cancer-related deaths.[4] Current existing therapies for K-RAS-driven NSCLC includes surgery, radiation therapy, and chemotherapy. One of the major limitation of all these therapies is severe toxicity, multidrug resistance, and poor survival outcomes.[5,6] Therefore, successful targeted therapy for K-RAS-driven NSCLC is considered to be clinically challenging.

Nanotechnology has opened up new avenues for more personalized treatment strategies for cancer therapy. The facile and reliable surface chemistry, better payloads makes these nanotechnology-based vehicles excellent candidates for drug delivery applications.[7−12] Nanoceria (NC), iron oxide nanoparticles (IONPs), polymeric nanoparticles (PNPs), quantum dots (QDs), gold nanoparticles (AuNPs), and carbon nanotubes (CNTs) have been used extensively for developing theranostic nanoplatforms.[13−18] Cerium oxide, a rare-earth metal has recently been shown to have diverse applications in cancer therapy due to unique redox property.[19−21] Several studies have examined the diverse role of antioxidant nanoceria as a therapeutic agent in cancer therapy because of its anti-invasive, radio protective, radio sensitizing, oxidant-mediated apoptosis, and antiangiogenic properties.[22−30]

Targeted delivery of chemotherapeutic drug cocktails specifically to the tumor site is becoming a popular choice for clinicians for effective cancer treatments. The unique combination of drug-carrying nanoplatform allows for the inhibition of separate tumorigenesis pathways. This strategy

Received: November 29, 2016
Revised: January 6, 2017
Accepted: January 12, 2017
Published: January 12, 2017

DOI: 10.1021/acs.molpharmaceut.6b01076
Mol. Pharmaceutics 2017, 14, 875−884

Scheme 1. Formulation of Functional and Biocompatible FNC: (1) Synthesis of PAA Polymer-Coated Cerium Oxide Nanoparticles (PNC) and (2) DiI Dye-Encapsulating PNC; (3) Propargylated Nanoceria Was Synthesized Using Carbodiimide Chemistry (4 and 5)[a]

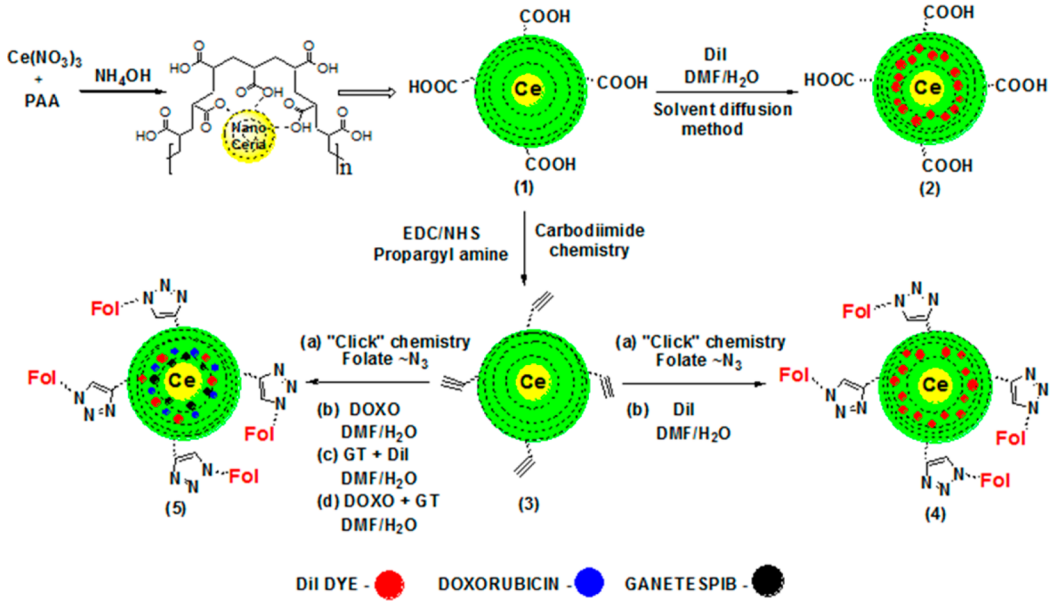

[a]"Click" chemistry was used to synthesize FNC, whereas a combination of drugs encapsulated using a solvent diffusion method.

could overcome severe side effects, multidrug resistance (MDR) of traditional chemotherapy and thereby obtain higher therapeutic efficacy. Considering the importance of cancer therapy, a new, dual-drug-carrying (Doxo and GT) functional nanoceria is proposed in this present study. Both drugs inhibit separate target mechanisms that are critical for tumor growth. The classical chemotherapeutic drug Doxo was selected in the present study, which is responsible for DNA damage and generation of ROS via redox-cycling.[31,32] To achieve synergistic treatment, GT, a second-generation Hsp90 inhibitor was chosen as another chemotherapeutic drug. Several studies have highlighted Hsp90 as an important target for cancer therapy. Its interaction with several client proteins including EGFR, RAF, and AKT leads to inhibition of multiple signaling cascades that are crucial for growth, differentiation, and survival of tumors.[33−38]

Herein, active targeting of NSCLC is achieved via folate conjugation of nanoceria which minimizes the off-target effects of the drug combination. Furthermore, the antioxidative property of nanoceria in the normal cells further boosts survival of healthy tissues and, therefore, minimizes side effects. Unique drug-cocktail-carrying nanoceria exhibits high anti-tumor activity for A549 cell line (NSCLC). Synergistic therapeutic effects are assessed via enhanced ROS, cytotoxicity, apoptosis, and migration assays as a result of codelivery of drug cocktail. Taken together, findings from the present study provide strong support for the clinical translation potential of our designer nanoceria formulations.

RESULTS AND DISCUSSION

Synthesis and Characterizations of Poly(acrylic acid) (PAA)-Coated Cerium Oxide Nanoparticles (PNC). The water-based alkaline precipitation method was followed for the synthesis of PAA-coated nanoceria (PNC), as previously reported.[39] The resulting yellow colored PNC solution was centrifuged to get rid of agglomerates and bigger size PNC and finally purified using dialysis technique (MWCO 6−8 kDa) (**1**, Scheme 1).[40] Next, modified solvent diffusion method was used to encapsulate optical lipophilic DiI dye in PNC (encapsulation efficiency, EE_{DiI} = 85%). In this case, the DiI dye-labeled carboxylated PNC (**2**, Scheme 1) would be used as a negative-control optical nanoprobe and to evaluate cytotoxicity of formulated PNC. For optical imaging, this kind of lipophilic dye is important because of its high extinction coefficient (ε > 125 000 cm^{-1} M^{-1}) and higher fluorescence emission (λ_{max} = 565 nm). In order to conjugate receptor-targeting molecules, first, propargyl amine was conjugated on the surface of PNC using standard EDC/NHS chemistry (**3**, Scheme 1). Briefly, carboxylic acid groups of PNC (2.0×10^{-3} mol) were conjugated with propargylamine (15×10^{-3} mol) using EDC (15×10^{-3} mol) and NHS (15×10^{-3} mol) in the presence of MES buffer (1×, pH = 6.0). This is an essential step to further conjugate our nanoparticles with azide-functionalized folic acid via "click chemistry" to target folate receptor expressing lung cancer cells (**4a−5a,** Scheme 1). This "click" reaction was performed in the presence of CuI as catalyst in a slightly basic PBS solution (pH = 8.0) of propargylated PNC suspension (2 mL, 1.5×10^{-3} mol) and azide-functionalized folic acid (Fol ~ N_3, 2×10^{-2} mol, see SI for detailed synthesis). The resulting folate-decorated nanoceria (FNC, 1.2×10^{-3} mol, **4a−5a**, Scheme 1) was purified using standard dialysis method (MWCO 6−8 kDa) and followed by DiI dye encapsulation as described earlier. The DiI dye-labeled FNC (**4b**, Scheme 1, 1.0×10^{-3} mol, EE_{DiI} = 83%) will be used for the targeted delivery of drugs to the folate receptor overexpressing cancer cells (positive nanoprobe). For therapeutic applications, Doxo and GT were encapsulated in FNC (**5b−5d**, Scheme 1, 1.0×10^{-3} mol, $EE_{Doxo/GT}$ = 75%) using solvent diffusion method. Finally, these nanoceria theranostics were purified using dialysis technique against PBS (pH = 7.4) solution. All functional nanoceria preparations were stored in 4 °C and found to be

DOI: 10.1021/acs.molpharmaceut.6b01076
Mol. Pharmaceutics 2017, 14, 875−884

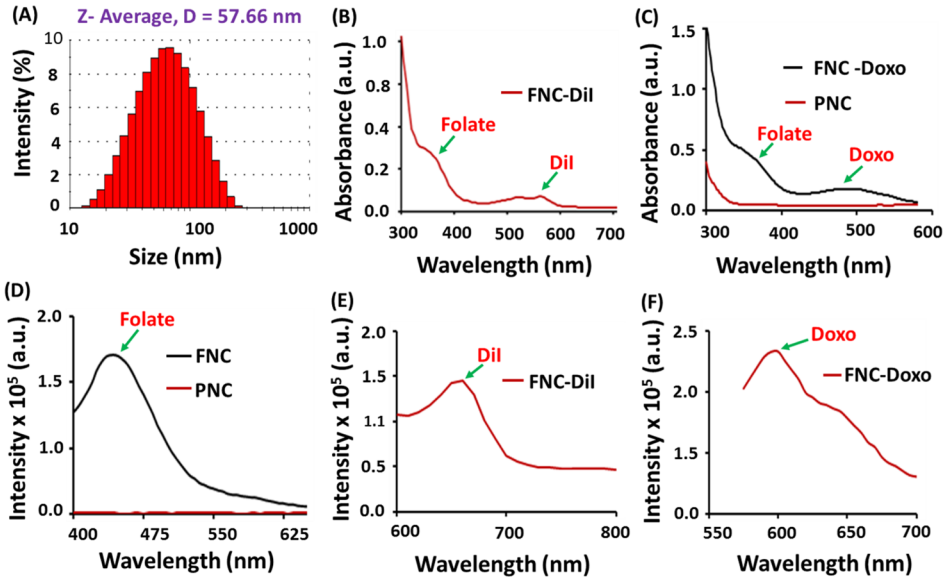

Figure 1. Characterizations of functional nanoceria. (A) Dynamic light-scattering experiment showed the formation of stable PNC with an average diameter of 57 ± 2 nm. UV−vis absorption spectra of (B) DiI-encapsulating FNC and (C) Doxo-encapsulating FNC showed the presence of folic acid and Doxo. Fluorescence emission spectra of (D) FNC, (E) DiI dye-encapsulating FNC, and (F) Doxo-encapsulating FNC further confirms for the successful synthesis.

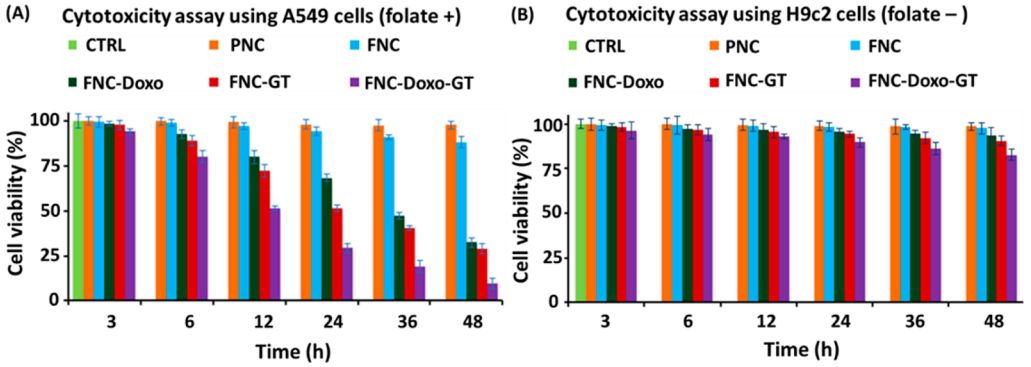

Figure 2. Determination of cytotoxicity of the formulated functional nanoceria using MTT assay. (A) More than 70% of A549 cells were dead within 24 h when incubated with the combination of drugs carrying nanoceria, whereas only 40% toxicity was observed with single drug delivered. However, more than 90% cells were found to be dead as a result of combination therapy after 48 h of incubation. (B) On the other hand, minimal toxicity was observed when functional nanoceria was incubated with H9c2 cells (FR−), suggesting for targeted delivery of drugs specifically to the tumor. A 1× PBS solution is used for the treatment of control cells. Average values of three measurements are depicted ± standard error.

stable in PBS (pH = 7.4) and in serum for longer period of time.

Characterizations of PAA Polymer-Coated Functional Nanoceria. The presence of the PAA coating on nanoceria is very crucial to make our nanoplatform stable, biocompatible and to efficiently encapsulate therapeutic drugs. Successful PAA coating and the presence of carboxylic acid functionality on nanoceria was confirmed by FT-IR spectroscopy (see SI, Figure S1). The presence of a band at 1710 cm^{-1} in FT-IR confirmed the presence of C═O stretching, indicating the successful coating of PAA polymer on nanoceria. The hydrodynamic diameter of synthesized PNC and FNC was found to be an average diameter of D = 57 ± 2 nm and D = 61 ± 3, respectively, measured through dynamic light-scattering experiment (Figure 1A and SI Figure S2). The overall surface charge of functional nanoceria preparations were measured by performing zeta-potential experiments and were found to be −32.9 mV and −25.2 mV for PNC and FNC (see SI, Figure S2), respectively. The successful encapsulation of optical dye and drugs inside the PAA coating of nanoceria were confirmed by UV−vis and fluorescence experiments using a high-throughput plate reader. The absorbance spectrum (Figure 1B) of the folate-decorated, DiI dye-encapsulating FNC **4** confirmed for the presence of both DiI dye (λ_{abs} = 555 nm) and folic acid (λ_{abs} = 352 nm). Similarly, the presence of Doxo in FNC (**5b**, Scheme 1) was confirmed by the UV−vis spectrum (λ_{abs} = 497 nm) as shown in Figure 1C. The effective folate conjugation and encapsulation of cargos were further confirmed by their corresponding fluorescence spectra (Fol: λ_{em} = 455 nm; DiI: λ_{em} = 675 nm; Doxo: λ_{em} = 595 nm, Figure 1D,E,F). The fluorescence maxima and hydrodynamic diameters of these functional nanoceria formulations remain unchanged (or minimal change) with a longer period of time, which is indicated for the synthesis of stable nanoceria formulations in phosphate buffer saline (PBS, pH = 7.4) and in serum.

Determination of Cytotoxicity of Functional Nanoceria. A series of in vitro cytotoxicity experiments were performed to evaluate the therapeutic efficacy of our drug-

DOI: 10.1021/acs.molpharmaceut.6b01076
Mol. Pharmaceutics 2017, 14, 875−884

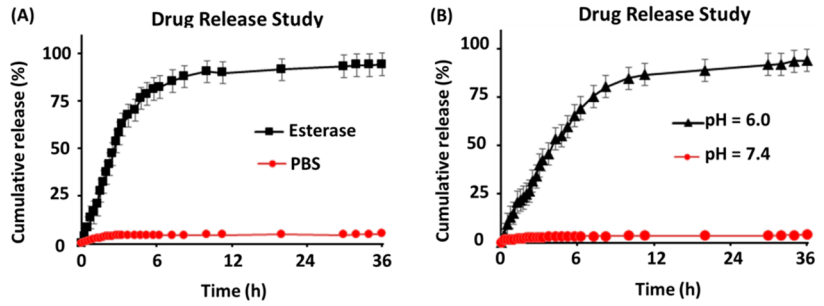

Figure 3. Drug-release profiles of FNC-Doxo using dialysis method. Release of Doxo (λ_{em} = 594 nm) was observed with time in the presence of (A) esterase enzyme and (B) in PBS at pH 6.0. However, the release of Doxo was minimal in PBS at pH 7.4 (Red line, A and B). The released Doxo emission was measured using plate reader at λ_{ex} = 497 nm. The results were recorded at λ_{em} = 594 nm and plotted in terms of % cumulative release. Average values of three measurements are depicted ± standard error.

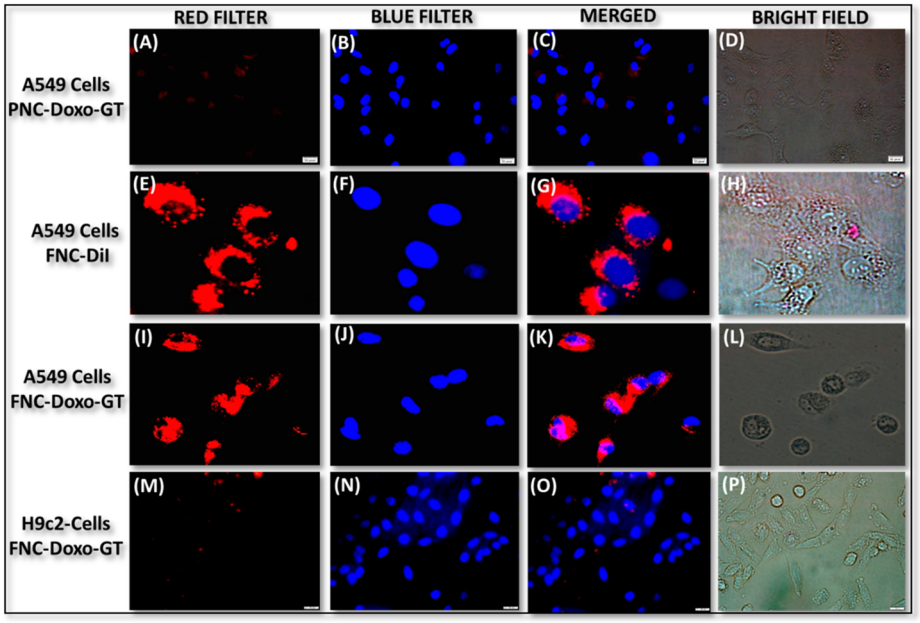

Figure 4. Representative fluorescence microscopic images of the in vitro cellular imaging and drug delivery experiments. (A–D) Minimal internalization was observed in the case of drug-loaded PNC, whereas (E–H) effective cellular internalization was observed with functional FNC (**4b**, Scheme 1). However, when drugs-loaded FNC (**5d**, Scheme 1) were incubated A549 cells, a substantial amount of cell death was observed (I–L). On the other hand, (M–P) minimal internalization was observed in healthy H9c2 cells, indicated for the targeted drug delivery. Nucleus stained with DAPI dye (blue).

encapsulated functional nanoceria using A549 (folate-positive) and H9c2 (folate-negative) cells. In these typical experiments, cells (2500 cells/well) in 96-well plate were incubated with various functional FNCs (35 μL, 1.0 × 10^{-3} mol) at 37 °C, followed by MTT incubation and finally data recorded at different time points. Comparable cellular toxicity was observed when incubated with single-drug-encapsulating FNC (either GT or Doxo), and more than 40% cells were found to be dead after 24 h of incubation. However, more than 70% cell death occurred within 24 h from the combination of drugs encapsulating nanoceria (FNC-Doxo-GT, **5d**, 1.0 × 10^{-3} mol, Scheme 1), which became more severe when continued (more than 90% cell death within 48 h of incubation, Figure 2A). On the other hand, functional nanoceria by itself (FNC) with no drugs showed minimal toxicity to the cancer cells as well as to the healthy cardiomyocytes, highlighting the biocompatibility of our nanoceria-based drug delivery system. No or minimal toxicity was observed when H9c2 cells (cardiomyocytes) were incubated with drug-loaded FNC (Figure 2B). This result is promising for reducing Doxo's potential lethal cardiotoxicity. Active targeting via FNC is one of the key aspect of our nanoplatform to achieve higher intracellular uptake of the drugs with minimal side effects to the healthy tissues. It is evident that as a result of synergistic effect, GT accelerates the cytotoxic action of Doxo, while minimizing Doxo's cardiotoxicity. Therefore, the targeted codelivery of drug cocktails using our functional nanoceria would offer an excellent combination therapy option for the treatment of undruggable NSCLC and other tumors.

Drug-Release Experiments of PAA Polymer-Coated Nanoceria. Next, drug-release studies were conducted to examine the ability of our PAA-coated nanoceria to release drug in the presence of an appropriate external environment, for example, low pH (tumor's intracellular environment) and esterase enzyme (to indicate biodegradability). It is crucial to determine timely release of cargos in order to evaluate therapeutic efficacy of our functional FNC. A dialysis technique was used in order to perform the drug-release experiment at 37 °C. Typically, 2 mL of Doxo-encapsulating FNC (1.0 × 10^{-3} mol) and 100 μL of porcine liver esterase (1 mM) were taken

DOI: 10.1021/acs.molpharmaceut.6b01076
Mol. Pharmaceutics 2017, 14, 875–884

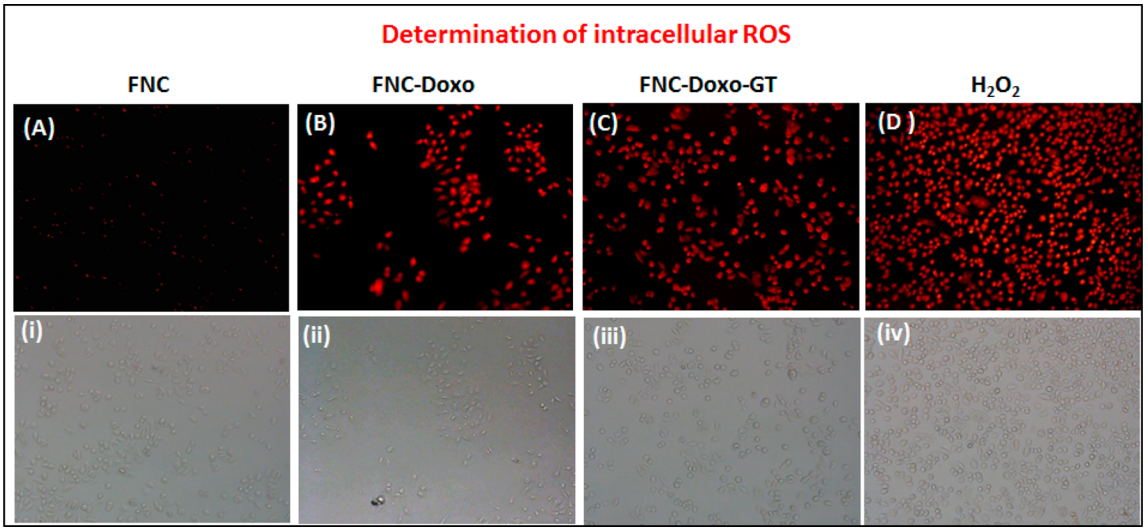

Figure 5. Determination of ROS generation. (A–D) Fluorescence microscopic images showing a relative increase in fluorescence from A549 cells because of the generation of increased amount of ROS after incubating with FNC, FNC-Doxo, FNC-Doxo-GT, and H_2O_2, respectively. Images (i–iv) are corresponding bright field images.

in a dialysis bag (MWCO 6–8 kDa) and dialyzed against 200 mL of DI water taken in a 250 mL beaker. In a timely fashion, 1 mL of solution from the outer chamber (250 mL beaker) was taken, and the fluorescence emission of this solution was measured at 594 nm using a high-throughput plate reader. As expected, a minimal amount of Doxo was released at the beginning of the dialysis; however, more than 50% of the encapsulating Doxo was released within 3 h of dialysis. In this case, the esterase enzyme was able to disrupt the PAA polymer from cerium oxide core, followed by the release of cargos. Within 6 h of incubation, more than 80% of the encapsulated drug was released, as shown in Figure 3A. Similarly, a drug-release experiment was performed in the presence of acidic PBS-buffered solution (pH = 6.0) by substituting the esterase enzyme. This experiment would demonstrate the drug-release capability of FNC inside the acidic microenvironment of the tumor. Within 12 h of incubation, more than 80% of the encapsulated drug was released, as shown in Figure 3B. In this case, the acidic pH hydrolyzes the coordinate bonding between cerium oxide and the carbonyl groups of PAA polymer, which resulted in PAA-coating disintegration and drug release. On the other hand, no or minimal drug release was observed in physiological pH 7.4. These observations indicated the stability of our functional FNC in physiological pH. These experiments further demonstrated that our functional nanoceria will deliver therapeutic drugs and imaging agents only in cancer cells, whereas they remain nontoxic to healthy tissues.

Fluorescence Microscopic Studies: Imaging and Treatment Monitoring of NSCLC. To evaluate the potential biomedical application of functional FNC, receptor-mediated internalization and selective therapeutic efficacy were assessed using fluorescence microscopy. We hypothesized that functional FNC would target folate receptors and internalize into folate receptor expressing tumors, while minimizing the cardiotoxicity of doxorubicin drug. In these in vitro experiments, lung cancer A549 cells were incubated with Doxo- and GT-encapsulating carboxylated nanoceria (nonfolate, PNC) for 24 h. Results showed no or minimal internalizations of drug-encapsulating PNC into A549 cells (Figure 4A-4D). This is due to the lack of interaction between carboxylated PNC and A549 cells. To validate effective internalization, optical dye DiI-encapsulating FNC (**4b**, Scheme 1) was incubated with A549 cells for 24 h. Interestingly, cellular internalization of FNC was observed as the cytoplasm was found to be red fluorescence in color due to the intracellular release of DiI dye (Figure 4E–H). To further demonstrate folate receptor-mediated internalizations, in a typical experiment, A549 cells were preincubated with free folic acid for 6 h before they were incubated with DiI-FNC for 24 h. Results showed minimal internalizations of FNC into the A549 cells (SI, Figure S3), indicating that the folate receptors were saturated with free folic acid and, therefore, receptor-mediated internalizations were minimized. When GT and Doxo-loaded FNC (**5d**, 1.0×10^{-3} mol, Scheme 1) were incubated with A549 cells for 24 h, tremendous change in cellular morphology and cell death were observed (Figure 4I–L). These results demonstrated the effective targeting and delivery of drugs effectively to cancer cells. These results were also validated with cytotoxic assays as demonstrated earlier (Figure 3). To prove our hypothesis for targeted delivery, we have considered folate-receptor-negative healthy cardiomyocyte cells (H9c2 cells). Dual-drug-encapsulating FNC (**5d**, Scheme 1) were incubated with H9c2 cells for 24 h and imaged under fluorescence microscope. As expected, results showed no or minimal internalizations into H9c2 cells, confirming tumor-targeting capability of our FNC, while minimizing toxicity to healthy tissues (Figure 4M–P). Taken together, these microscopic results indicated for the tremendous possibility of our newly designed drug-cocktail-encapsulating FNC to be used as targeted drug delivery system in clinical settings.

Intracellular Reactive Oxygen Species (ROS) Detection Assay. Enhancing ROS levels selectively in the cancer cells is a relatively newer approach to achieve better anticancer therapy. Dihydroethidium (DHE), a fluorescent dye, was used to determine the generation of ROS. In the presence of reactive oxygen species, DHE is oxidized into 2-hydroxyethidium and fluoresces red after intercalating within the nuclei. Previous studies have shown ROS generation via redox cycling as one of the main mechanisms by which doxorubicin exerts its antitumor activity.[22] To determine whether ganetespib (GT) synergizes the ROS production of doxorubicin, A549 cells were

DOI: 10.1021/acs.molpharmaceut.6b01076
Mol. Pharmaceutics 2017, 14, 875–884

treated with a combination of drugs, doxorubicin (Doxo), and GT-carrying FNC (**5d**, 1.0×10^{-3} mol, Scheme 1). In these experiments, four Petri dishes of A549 cells (10 000/well) were treated with different functional FNCs and others: (1) FNC without any drug, (2) FNC with only doxorubicin (FNC-Doxo), (3) FNC with drug cocktail (FNC-Doxo-GT) and (4) H_2O_2 (positive control). After 6 h of treatment, cells were stained with highly cell permeable cytosolic probe dihydroethidium (DHE) for 30 min. Cells treated with FNC showed minimal red fluorescence due to production of limited ROS stress (Figure 5A-i). In contrast, FNC-Doxo elevated the ROS level significantly as indicated by the 4-fold higher fluorescence intensity (Figure 5B-ii). This further demonstrated the doxorubicin-induced cytotoxicity via redox-cycling. Next, to verify the synergistic effect of GT on Doxo's ROS production, we have treated A549 cells with FNC-Doxo-GT (**5d**, 1.0×10^{-3} mol, Scheme 1). Interestingly, this led to the dramatic enhancement of ROS levels as indicated in Figure 5C-iii. This further validates our hypothesis that combination of ganetespib improves the therapeutic efficacy of doxorubicin by triggering ROS generation. In addition, the numerical data of fluorescent intensities from each fluorescence microscopic images were calculated using the commercially available ImageJ software and the histogram profiles exhibited for the increased levels of ROS generation, as shown in Figure 6. One of the

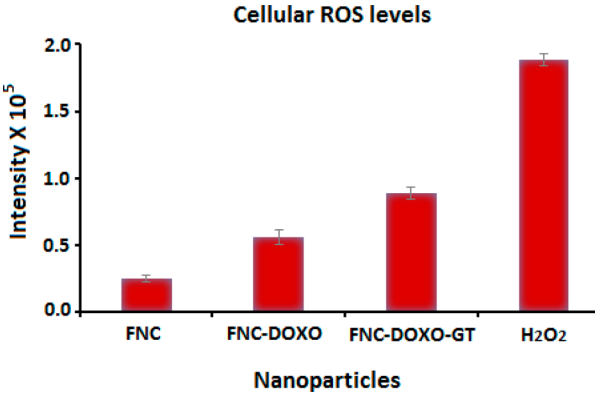

Figure 6. Numerical data were calculated from corresponding ROS images using ImageJ software. Results showed relatively higher fluorescence from the FNC-Doxo-GT-treated A549 cells because of the presence of increased amount of ROS, as expected. Average values of three measurements are depicted ± standard error.

mainstays in cancer therapy is to employ a combination of drugs to achieve better therapeutic outcome. Our present findings from the ROS assay provides a strong rationale of exploring combination therapy for the treatment of NSCLC using nanoceria.

Detection of Apoptotic and Necrotic Events on NSCLC. Having identified ROS production as a result of functional FNC treatment, next we wanted to elucidate the correlation between ROS generation and apoptosis induction. To investigate the mechanism, in a typical experiment, A549 cells were exposed to the FNC, FNC-Doxo, and FNC-Doxo-GT (1.0×10^{-3} mol) for 48 h. Additionally, to differentiate between early and late apoptotic, and necrotic cells, conventional fluorescence microscopic studies were performed after treatment with AnnexinV-FITC and ethidium homodimer, the apoptotic and necrotic cell staining dyes, respectively. Viable and healthy cells remain unstained, as shown in Figure 7A-i in the case of treatment with FNC with no drug and due to the absence of any cell death mechanism. Encapsulation of doxorubicin leads to early and late apoptosis, as exhibited by AnnexinV-FITC and ethidium homodimer staining pattern (major green spots for apoptotic cells and fewer red spots for necrotic events, Figure 7B-ii). In contrast, upon combination drug treatment, A549 cells exhibited enhanced ethidium homodimer staining, indicated for cell death via necrotic pathway (major red spots for necrotic cells: Figure 7C-iii). Quantitative analysis of these results are calculated using ImageJ software and presented in SI Figure S4. These further confirm that GT treatment accelerates the apoptosis induction of doxorubicin, leading to extensive loss in membrane integrity that eventually results in cell death via necrosis. On the basis of these results, it is evident that ganetespib provides superior therapeutic efficacy by markedly enhancing the antitumor activity of doxorubicin. Taken together, our results suggest that combination of ganetespib with classical chemotherapeutic drug doxorubicin might provide a better synergistic antitumor response for the treatment of NSCLC. We also suggest that the development of functional nanoceria formulation with strong evidence for better antitumor response would be an ideal drug delivery system for the targeted combination therapy of NSCLC and other tumors.

Migration Assay. Metastasis is known to be a key feature for the malignancy of NSCLC. To assess whether nanoceria carrying drug cocktail can inhibit the migration of highly metastatic A549 cell line, we performed transwell migration assays. In these experiments, serum-starved A549 cells were treated with functional FNC (1.0×10^{-3} mol) and seeded in the upper invasion chamber, followed by incubation for 24 h. Our results showed that A549 cells migrated from the upper to the lower chamber (feeder tray) containing medium with 10% FBS, when treated with FNC with no drugs (CTRL, Figure 8). However, when starved A549 cells were treated with nanoceria carrying a combination of drugs, migration ability decreased significantly, as reflected by the change in the fluorescence intensity (FNC-Doxo-GT, Figure 8). Taken together, our current findings demonstrated that functional nanoceria carrying doxorubicin and ganetespib might play an important role in preventing lung cancer metastasis.

EXPERIMENTAL SECTION

Materials. Polyacrylic acid (PAA), 2-morpholinoethanesulfonic acid (MES), 1-ethyl-3-(3-(dimethylamino)-propylcarbodiimide hydrochloride (EDC), propargylamine (PA), *N*,*N*′-dimethyl sulfoxide (DMSO), 3-(4,5-dimethylthiazol-2-yl)-2,5-diphenyltetrazolium bromide (MTT), chloropropylamine, and *N*,*N*′-dimethylformamide (DMF) were purchased from Sigma-Aldrich and used as received. Near infrared DiI dye and 4,6-diamidino-2-phenylindole (DAPI) dye were purchased from Invitrogen. Cerium nitrate hexahydrate, *N*-hydroxy succinimide (NHS), tetrahydrofuran, acetonitrile, sodium azide, ammonium hydroxide, ethanol, folic acid, isopropanol, and MES sodium salt were purchased from ACROS organics and used without further purification. Dialysis membranes were received from spectrum laboratories. Dihydroethidium (DHE) was obtained from Cayman chemical, whereas H_2O_2 and para-formaldehyde were received from electron microscopy sciences. Fetal bovine serum (FBS) and 5× Annexin V binding buffer were purchased from BD Biosciences, whereas ganetespib, isopropyl alcohol, apoptosis and necrosis quantification kit (FITC-Annexin V, Ethidium

DOI: 10.1021/acs.molpharmaceut.6b01076
Mol. Pharmaceutics 2017, 14, 875−884

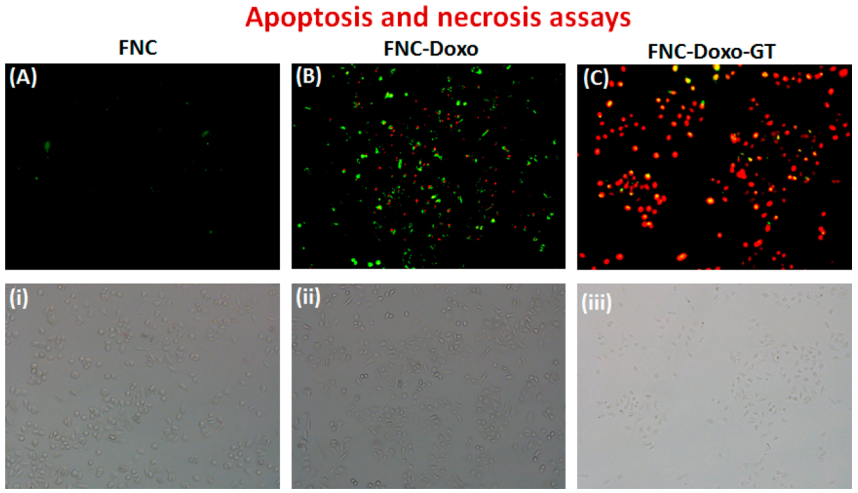

Figure 7. Detection of apoptotic and necrotic cell death by fluorescence microscopy using annexinV-FITC and ethidium homodimer III. (A) Healthy cells emitted almost no fluorescence representing early apoptotic cells. (B) Apoptotic cells emitted green fluorescence after treatment with FNC-Doxo. (C) Necrotic cells emitted red fluorescence when treated with FNC with combination of drugs. (i), (ii), and (iii) represents corresponding bright field images.

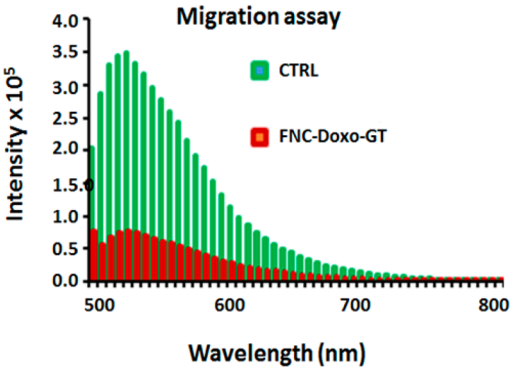

Figure 8. Assessment for the inhibition of migration of highly metastatic A549 cells via migration assay. Control cells (green lines) incubated with FNC with no drug showed maximum invasion, whereas a combination of drug-carrying-FNC-treated A549 cells (red lines) showed minimal migration. The sample average value of three successive measurements is presented in both CTRL and FNC-Doxo-GT experiments.

homodimer III) were obtained from Biotium. Migration assay kit was purchased from Millipore. Rat cardiomyocytes (H9c2 cells), A549 cells (NSCLC), DMEM, and F12K cell culture media were purchased from ATCC (U.S.A.).

Synthesis of Poly(acrylic acid)-Coated Nanoceria 1 (PNC). Water-dispersible PNC were synthesized using a previously reported water-based alkaline precipitation method.[39] Briefly, two different solutions were prepared: cerium nitrate (0.901 g) in 2.5 mL of deionized (DI) water (solution 1) and poly(acrylic acid) (0.905 g) in 10 mL of DI water (solution 2). Solution 1 was added to 30% ammonium hydroxide solution (30 mL), stirred at room temperature, and followed by addition of solution 2. Color changed from brown to dark brown within 5 min of stirring and became deep yellow after 24 h, which indicates the preparation of stable nanoceria. The reaction mixture was centrifuged three times (20 min each at 3000 rpm) to get rid of agglomerates and bigger size PNC. Finally, the product was purified by dialysis technique using a dialysis bag of molecular weight cutoff (MWCO) 6−8K against DI water and finally with phosphate buffer saline (PBS, pH = 7.4). The purified PNC (2.0×10^{-3} mol) was stored at 4 °C for further characterizations. Successful coating of PAA on nanoceria was characterized by Fourier Transform Infra-Red (FT-IR) spectroscopy (SI, Figure S1), overall size and surface charge were measured using dynamic light-scattering (DLS) technique (SI, Figure S2).

Synthesis of Propargylated PNC, 3: Carbodiimide Chemistry. To synthesize propargylated PNC, four different solutions were prepared: (1) 3 mL PNC (2.0×10^{-3} mol) in 1 mL of PBS, pH 7.4, (2) NHS (15×10^{-3} mol) in 200 μL of MES buffer (0.1 M), pH = 6.0, (3) EDC (15×10^{-3} mol) in 200 μL of MES buffer (0.1 M), pH = 6.0, and (4) propargylamine (15×10^{-3} mol) in 250 μL of DMSO. The EDC solution was immediately added to PNC solution and followed by addition of NHS solution, after brief mixing. This reaction mixture was incubated for an additional 3 min before dropwise addition of solution 4, at room temperature. The reaction was continued for 4−6 h at room temperature. The final alkynated PNC was purified against PBS (pH = 7.4) using the dialysis method (MWCO 6−8K) to get rid of unreacted reagents.

Synthesis of Folate-Conjugated PNC (FNC, 4a and 5a): "Click" Chemistry. To a solution of propargylated PNC suspension (2 mL, 1.5×10^{-3} mol) in bicarbonate buffer (pH = 8.0) and azide-functionalized folic acid (Fol ~ N_3, 2×10^{-2} mol, See SI for detailed synthesis) in DMF, 5 μL of CuI catalyst (1×10^{-3} mmol) in DMF was added and incubated on a table mixer for overnight at room temperature. The resulting product was purified using the dialysis technique. The purified FNC (1.2×10^{-3} mol) was stored at 4 °C for further characterizations.

Encapsulation of DiI Dye (2 and 4b): Solvent Diffusion Method. To 1 mL of nanoceria (PNC or FNC) suspension, DiI dye (1 μL of 1 μM DiI dye in 100 μL of DMSO) was added dropwise with continuous stirring. The resulting solution was dialyzed against PBS (pH = 7.4) for 2 h. Successful encapsulation of DiI was confirmed using UV−vis and fluorescence spectrophotometric analyses (Figure 1). The purified dye-labeled nanoceria suspensions (1.0×10^{-3} mol) were stored at 4 °C for further studies.

DOI: 10.1021/acs.molpharmaceut.6b01076
Mol. Pharmaceutics 2017, 14, 875−884

Coencapsulation of Doxorubicin (Doxo) and Ganetespib (GT). Using a similar solvent diffusion method, a combination of drugs or drug and dye were coencapsulated. Briefly, a solution of either GT and DiI or GT and Doxo (2 μM of drug in 100 μL DMSO) was slowly added to 1 mL of vortexing FNC suspension, followed by overnight incubation at 4 °C. The drug-encapsulating functional FNC suspensions were dialyzed against PBS (pH = 7.4) for 2 h. The purified functional FNC suspension was stored at 4 °C for further studies.

Characterizations of Functional Nanoceria. *Fourier-Transform Infra-Red Spectroscopy (FT-IR).* PerkinElmer's Spectrum Two FT-IR spectrometer was used for FT-IR measurement. PNC suspension was vacuum-dried on a Petri dish to obtain the powder form. FT-IR spectra of PAA polymer and PNC were recorded and compared. The presence of FT-IR stretching band at 1710 cm^{-1} for the PAA polymer's carboxylic acid carbonyl group confirmed for the formation of PAA polymer coating on PNC (SI, Figure S1).

Dynamic Light-Scattering Experiments (DLS). The average size distribution and surface charge of functional nanoceria were obtained using the dynamic light-scattering technique. Malvern's Nano-ZS90 zetasizer was used for these experiments. The average diameters of PNC and FNC were found to be 57.66 and 61.65 nm, respectively. The zeta potentials of PNC and FNC were −32.9 and −25.2 mV, respectively (SI, Figure S2).

Spectrophotometric Analysis. UV−vis and fluorescence spectra of functional nanoceria were recorded using TECAN's infinite M200 PRO high throughput plate reader. Presence of folic acid in FNC was confirmed by UV−vis (λ_{abs} = 352 nm) and fluorescence emission spectra (λ_{em} = 455 nm). Successful encapsulation of Doxo was determined by UV−vis (λ_{abs} = 497 nm) and fluorescence emission spectra (λ_{em} = 595 nm). Finally, the presence of DiI dye was confirmed by UV−vis (λ_{abs} = 555 nm) and fluorescence emission spectra (λ_{em} = 675 nm).

Cytotoxicity Studies using MTT Assay. To determine the potential time-dependent cytotoxicity, two different cell lines, lung carcinoma (A549 cells) and cardiomyocytes (H9c2 cells), were used. Cells were seeded in 96-well plates at a density of 2500 cells per well and treated with various functional FNCs (1.0×10^{-3} mol) at 37 °C for different time points. Each well was washed thrice with 1× PBS and then incubated with 30 μL of 5 mM MTT solution. After 4−6 h of incubation, the resulting formazan crystals (purple color) were dissolved in acidic isopropyl alcohol (75 μL), and the absorbance at 570 nm was recorded using TECAN's microplate reader. These assays were carried out in triplicate, and the results were reported in Figure 2.

Drug-Release Studies via Dynamic Dialysis Technique. The in vitro drug-release studies were carried out at 37 °C using esterase enzyme and at low pH. We have incubated 2 mL of functional nanoceria with a 100 μL of porcine liver esterase (1 mM) inside a dialysis bag of molecular weight cutoff 6000−8000 Da, and was placed in a PBS solution (200 mL, pH = 7.4). The amount of drug molecules released from the functional FNC-Doxo (1.0×10^{-3} mol) into the PBS solution was determined at regular time intervals by taking 1 mL aliquots from the PBS solution and replacing the same with PBS solution. Fluorescence emission was measured at 494 nm for doxorubicin. The same procedure was followed with 100 μL of acidic PBS buffer (pH 6.0) at 37 °C. A standard calibration curve was used to calculate the concentration of the drug released, and the cumulative drug release versus time was calculated using the following eq (Figure 3). Cumulative release (%) = $(\text{guest})_t/(\text{guest})_{total} \times 100$.

Fluorescence Imaging: Cellular Internalization and Cancer Treatment. The lung carcinoma A549 cells were seeded into 12-well plate and once cells become 75% confluent, they were treated with corresponding PNC-Doxo-GT, FNC-DiI and FNC-Doxo-GT (1.0×10^{-3} mol) for 24 h in a humidified incubator (37 °C, 5% CO_2). The cells were washed thrice with 1× PBS (pH = 7.4) and were fixed with 4% formaldehyde solution for 15 min at room temperature. The cells were then washed twice with 1× PBS before treating with 6-diamidino-2-phenylindole (DAPI, 5 mg/mL) dye for nuclei staining. Cells were washed with 1× PBS and optical images were taken using fluorescence microscope (Olympus IX73) and results were shown in Figure 4A−L. For control experiment, H9c2 cells were treated with FNC-Doxo-GT (1.0×10^{-3} mol), and the results were shown in Figure 4M−P.

ROS Detection Assay. Cells were seeded into different Petri-dishes at a density of 10 000 cells per well and treated with 50 μL of various nanoceria preparations (FNC, FNC-Doxo, FNC-Doxo-GT, H_2O_2, 1.0×10^{-3} mol). After 6 h of incubation at 37 °C, cells were washed twice with 1× PBS. Then, 20 μL of DHE fluorescent probe was added to each well and incubated for 30 min at room temperature, followed by washing the cells twice with 1× PBS. Subsequently, cells were fixed with 1 mL of 4% paraformaldehyde. After fixation, cells were washed with 1× PBS, stored with 2 mL of PBS in each well, and the optical images were taken using fluorescence microscope (Figure 5).

Determination of ROS using ImageJ Software. Using ROS fluorescence images, the amount of ROS was quantified using commercial ImageJ software. A particular cell from each treated FNCs condition was selected to get a stack of values for the area, integrated density, and mean fluorescence of background readings. Using the CTCF formula, the corrected total cell fluorescence (CTCF) for each condition was calculated, and the results were shown in Figure 6. CTCF = integrated density − (area of selected cell × mean fluorescence of background readings).

Apoptosis and Necrosis Assay. The apoptosis and necrosis assays were carried out using apoptosis and necrosis quantification kit obtained from Biotium and using fluorescence microscopy. First, A549 cells were seeded into three different Petri-dishes at a density of 10 000 cells per well. Next, cells were treated with different preparations (FNC, FNC-Doxo, and FNC-Doxo-GT, 1.0×10^{-3} mol) and incubated for 48 h. Cells were washed thrice with 1× PBS and then fixed with 4% formaldehyde solution for 15 min at room temperature. Later, the cells were stained with two different dyes, 5 μL of FITC-annexin buffer, and 5 μL of ethidium dimer III and incubated for 15 min. After the cells were washed thrice with 1× PBS, cells were covered with 1× binding buffer. Multiple fluorescence images were taken using two filters: (1) FITC for green fluorescence, representing apoptosis, and (2) ethidium homodimer III for red fluorescence, indicating necrosis (Figure 7).

Migration or Invasion Assay. Chemicon QCM 96-well cell-migration assay kit from Millipore was used to evaluate the migration of A549 cells in the presence of functional nanoparticles. Briefly, serum-starved A549 cells were cultured for 24 h. Next, A549 cells were harvested and treated with the functional nanoceria (FNC-Doxo-GT, 1.0×10^{-3} mol) and PBS (control). Following treatment, cells were seeded into the upper chamber (transwell, invasion chamber), coated with type

DOI: 10.1021/acs.molpharmaceut.6b01076
Mol. Pharmaceutics 2017, 14, 875−884

I collagen. The lower chamber (feeder tray) contained medium with 10% FBS, and the whole setup was placed in the incubator for an additional 24 h to allow migration. Then, the migratory cells were dislodged completely from the invasion chamber and incubated with cell detachment buffer for 30 min. Finally, diluted solution of CYQuant cell lysis buffer was added to stain the migratory cells and was read on a fluorescent plate reader. Fluorescence intensity was measured at an emission wavelength of 520 nm (Figure 8).

CONCLUSIONS

In conclusion, we have successfully synthesized functional nanoceria as a drug-delivery vehicle with a unique drug cocktail for the treatment of NSCLC. Folate-decorated nanoceria were formulated for the targeted delivery of combination of drugs, Doxo and GT. Resulting functional nanoceria demonstrated excellent drug payload as reflected by the encapsulation studies, enhanced stability, reduced systemic toxicity, and higher therapeutic efficacy. As a result of combination therapy, more than 80% of NSCLC cells were dead within 48 h of incubation. Results indicated cotreatment with GT supplements the classical chemotherapeutic efficacy of Doxo, as confirmed by cell-based experiments including MTT and apoptosis assays. Furthermore, ROS studies indicated that GT synergizes and enhances the therapeutic efficacy of Doxo via ROS production, while minimizing the potential cardiotoxicity of doxorubicin drug. Apoptosis and necrosis assays further indicated the synergistic effect of GT on Doxo's therapeutic action. In addition, a migration assay validated the important role of this combination therapy approach in preventing lung cancer metastasis. Therefore, our current approach of delivering GT and Doxo using functional nanoceria may offer a robust nanoplatform for the targeted treatment of clinically challenging K-RAS driven NSCLC.

ASSOCIATED CONTENT

Supporting Information

The Supporting Information is available free of charge on the ACS Publications website at DOI: 10.1021/acs.molpharmaceut.6b01076.

Synthesis and characterizations of folic acid derivatives; functional FNC; control experiments for cellular internalizations; FT-IR spectra; size and ζ-potential studies (PDF)

AUTHOR INFORMATION

Corresponding Author

*E-mail: ssantra@pittstate.edu.

ORCID

Santimukul Santra: 0000-0002-5047-5245

Notes

The authors declare no competing financial interest.

ACKNOWLEDGMENTS

This work is supported by K-INBRE P20GM103418, ACS PRF 56629-UNI7, and PSU polymer chemistry startup fund (all funding to S.S.).

REFERENCES

(1) Jemal, A.; Center, M. M.; DeSantis, C.; Ward, E. M. Global patterns of cancer incidence and mortality rates and trends. *Cancer Epidemiol., Biomarkers Prev.* **2010**, *19*, 1893−1907.

(2) Siegel, R.; Ma, J.; Zou, Z.; Jemal, A. Cancer statistics, 2014. *Ca-Cancer J. Clin.* **2014**, *64*, 9−29.

(3) American Cancer Society. *Cancer Facts & Figures 2016*; American Cancer Society: Atlanta, GA, 2016.

(4) Acquaviva, J.; Smith, D. L.; Sang, J.; Friedland, J. C.; He, S.; Sequeira, M.; Zhang, C.; Wada, Y.; Proia, D. A. Targeting KRAS-mutant non-small cell lung cancer with the Hsp90 inhibitor ganetespib. *Mol. Cancer Ther.* **2012**, *11*, 2633−2643.

(5) Ramalingam, S.; Belani, C. Systemic chemotherapy for advanced non-small cell lung cancer: recent advances and future directions. *Oncologist* **2008**, *13* (Suppl1), 5−13.

(6) Grossi, F.; Kubota, K.; Cappuzzo, F.; de Marinis, F.; Gridelli, C.; Aita, M.; Douillard, J. Y. Future scenarios for the treatment of non-small cell lung cancer: focus on taxane-containing regimens. *Oncologist* **2010**, *15*, 1102−1112.

(7) van Vlerken, L. E.; Amiji, M. M. Multi-functional polymeric nanoparticles for tumour-targeted drug delivery. *Expert Opin. Drug Delivery* **2006**, *3*, 205−216.

(8) Santra, S.; Kaittanis, C.; Perez, J. M. Aliphatic hyperbranched polyester: a new building block in the construction of multifunctional nanoparticles and nanocomposites. *Langmuir* **2010**, *26*, 5364−5373.

(9) Santra, S.; Kaittanis, C.; Grimm, J.; Perez, J. M. Drug/dye-loaded, multifunctional iron oxide nanoparticles for combined targeted cancer therapy and dual optical/magnetic resonance imaging. *Small* **2009**, *5*, 1862−1868.

(10) Singh, S. Nanomedicine-nanoscale drugs and delivery systems. *J. Nanosci. Nanotechnol.* **2010**, *10*, 7906−7918.

(11) Santra, S.; Kaittanis, C.; Perez, J. M. Cytochrome c encapsulating theranostic nanoparticles: A novel bifunctional system for targeted delivery of therapeutic membrane-impermeable proteins to tumors and imaging of cancer therapy. *Mol. Pharmaceutics* **2010**, *7*, 1209−1222.

(12) Singh, R.; Nalwa, H. S. Medical applications of nanoparticles in biological imaging, cell labeling, antimicrobial agents, and anticancer nanodrugs. *J. Biomed. Nanotechnol.* **2011**, *7*, 489−503.

(13) Lin, W.; Huang, Y. W.; Zhou, X. D.; Ma, Y. Toxicity of cerium oxide nanoparticles in human lung cancer cells. *Int. J. Toxicol.* **2006**, *25*, 451−457.

(14) Baker, C. H. Harnessing cerium oxide nanoparticles to protect normal tissue from radiation damage. *Transl. Cancer Res.* **2013**, *2*, 343−358.

(15) McCarthy, J. R.; Perez, J. M.; Bruckner, C.; Weissleder, R. Polymeric nanoparticle preparation that eradicates tumors. *Nano Lett.* **2005**, *5*, 2552−2556.

(16) Santra, S.; Jativa, S. D.; Kaittanis, C.; Normand, G.; Grimm, J.; Perez, J. M. Gadolinium-encapsulating iron oxide nanoprobe as activatable NMR/MRI contrast agent. *ACS Nano* **2012**, *6*, 7281−7294.

(17) Qian, Y.; Qiu, M.; Wu, Q.; Tian, Y.; Zhang, Y.; Gu, N.; Li, S.; Xu, L.; Yin, R. Enhanced cytotoxic activity of cetuximab in EGFR-positive lung cancer by conjugating with gold nanoparticles. *Sci. Rep.* **2014**, *4*, Article No. 7490.

(18) Brown, S. D.; Nativo, P.; Smith, J. A.; Stirling, D.; Edwards, P. R.; Venugopal, B.; Flint, D. J.; Plumb, J. A.; Graham, D.; Wheate, N. J. Gold nanoparticles for the improved anticancer drug delivery of the active component of oxaliplatin. *J. Am. Chem. Soc.* **2010**, *132*, 4678−4684.

(19) Chen, J.; Patil, S.; Seal, S.; McGinnis, J. F. Rare earth nanoparticles prevent retinal degeneration induced by intracellular peroxides. *Nat. Nanotechnol.* **2006**, *1*, 142−150.

(20) Tarnuzzer, R. W.; Colon, J.; Patil, S.; Seal, S. Vacancy engineered ceria nanostructures for protection from radiation-induced cellular damage. *Nano Lett.* **2005**, *5*, 2573−2577.

(21) Rzigalinski, B. A.; Bailey, D.; Chow, L.; Kuiry, S. C.; Patil, S.; Merchant, S.; Seal, S. Cerium oxide nanoparticles increase the lifespan

DOI: 10.1021/acs.molpharmaceut.6b01076
Mol. Pharmaceutics 2017, 14, 875−884

of cultured brain cells and protect against free radical and mechanical trauma. *FASEB J.* **2003**, *17*, A606.
(22) Sack, M.; Alili, L.; Karaman, E.; Das, S.; Gupta, A.; Seal, S.; Brenneisen, P. Combination of conventional chemotherapeutics with redox-active cerium oxide nanoparticles-a novel aspect in cancer therapy. *Mol. Cancer Ther.* **2014**, *13*, 1740−1749.
(23) Asati, A.; Santra, S.; Kaittanis, C.; Nath, S.; Perez, J. M. Oxidase-like activity of polymer-coated cerium oxide nanoparticles. *Angew. Chem., Int. Ed.* **2009**, *48*, 2308−2312.
(24) Dowding, J. M.; Das, S.; Kumar, A.; Dosani, T.; McCormack, R.; Gupta, A.; Sayle, T. X.; Sayle, D. C.; von Kalm, L.; Seal, S.; Self, W. T. Cellular interaction and toxicity depend on physicochemical properties and surface modification of redox-active nanomaterials. *ACS Nano* **2013**, *7*, 4855−4868.
(25) Desmouliere, A.; Guyot, C.; Gabbiani, G. The stroma reaction myofibroblast: a key player in the control of tumor cell behavior. *Int. J. Dev. Biol.* **2004**, *48*, 509−517.
(26) Yuan, H.; Miao, J.; Du, Y. Z.; You, J.; Hu, F. Q.; Zeng, S. Cellular uptake of solid lipid nanoparticles and cytotoxicity of encapsulated paclitaxel in A549 cancer cells. *Int. J. Pharm.* **2008**, *348*, 137−145.
(27) Nelson, M. E.; Loktionova, N. A.; Pegg, A. E.; Moschel, R. C. 2-Amino-O4-benzylpteridine derivatives: potent inactivators of O6-alkylguanine-DNA alkyltransferase. *J. Med. Chem.* **2004**, *47*, 3887−3891.
(28) Weissleder, R.; Ntziachristos, V. Shedding light onto live molecular targets. *Nat. Med.* **2003**, *9*, 123−128.
(29) Lin, W.; Huang, Y.; Zhou, X.; Ma, Y. Toxicity of cerium oxide nanoparticles in human lung cancer cells. *Int. J. Toxicol.* **2006**, *25*, 451−457.
(30) Giri, S.; Karakoti, A.; Graham, R. P.; Maguire, J. L.; Reilly, C. M.; Seal, S.; Rattan, R.; Shridhar, V. Nanoceria: a rare-earth nanoparticle as a novel anti-angiogenic therapeutic agent in ovarian cancer. *PLoS One* **2013**, *8*, e54578.
(31) Minotti, G.; Menna, P.; Salvatorelli, E.; Cairo, G.; Gianni, L. Anthracyclines: molecular advances and pharmacologic developments in antitumor activity and cardiotoxicity. *Pharmacol. Rev.* **2004**, *56*, 185−229.
(32) Du, C.; Deng, D.; Shan, L.; Wan, S.; Cao, J.; Tian, J.; Achilefu, S.; Gu, Y. A pH-sensitive doxorubicin prodrug based on folate-conjugated BSA for tumor-targeted drug delivery. *Biomaterials* **2013**, *34*, 3087−3097.
(33) Hahn, J. S. The Hsp90 chaperone machinery: from structure to drug development. *BMB Rep.* **2009**, *42*, 623−630.
(34) Whitesell, L.; Lindquist, S. L. HSP90 and the chaperoning of cancer. *Nat. Rev. Cancer* **2005**, *5*, 761−772.
(35) Trepel, J.; Mollapour, M.; Giaccone, G.; Neckers, L. Targeting the dynamic HSP90 complex in cancer. *Nat. Rev. Cancer* **2010**, *10*, 537−549.
(36) Banerji, U. Heat shock protein 90 as a drug target: some like it hot. *Clin. Cancer Res.* **2009**, *15*, 9−14.
(37) Neckers, L. Heat shock protein 90: the cancer chaperone. *J. Biosci.* **2007**, *32*, 517−530.
(38) Xu, W.; Neckers, L. Targeting the molecular chaperone heat shock protein 90 provides a multifaceted effect on diverse cell signaling pathways of cancer cells. *Clin. Cancer Res.* **2007**, *13*, 1625−1629.
(39) Perez, J. M.; Asati, A.; Nath, S.; Kaittanis, C. Synthesis of biocompatible dextran-coated nanoceria with pH-dependent antioxidant properties. *Small* **2008**, *4*, 552−556.
(40) Asati, A.; Santra, S.; Kaittanis, C.; Perez, J. M. Surface-charge-dependent cell localization and cytotoxicity of cerium oxide nanoparticles. *ACS Nano* **2010**, *4*, 5321−5331.

DOI: 10.1021/acs.molpharmaceut.6b01076
Mol. Pharmaceutics 2017, 14, 875−884